EFFECTS OF SWELLING ON BRAIN TISSUE MECHANICAL PROPERTIES BY INDENTATION

BY

PETER SHYU

THESIS

Submitted in partial fulfillment of the requirements
for the degree of Master of Science in Mechanical Engineering
in the Graduate College of the
University of Illinois at Urbana-Champaign, 2018

Urbana, Illinois

Adviser:

Professor Yuhang Hu

ABSTRACT

Constructing more in-depth models of the brain's behavior has gained significant attention in recent years, particularly for the goal of modeling brain injury and function. Mechanical studies have improved in effectiveness with the development of more standard testing protocols and the contribution of mechanistic models to understanding the brain's behavior. Due to the complexity of the brain's structure and pathophysiology of diseases and conditions related to swelling, studies have mainly focused on identifying the mechanisms underlying brain tissue swelling. Most commonly, magnetic resonance imaging techniques have been used, particularly with the development of magnetic resonance elastography, to study swelling *in vivo*. However, localized testing on *in vitro* tissue slices have become useful alternatives as models of study with atomic force microscopy and nanoindentation. Here, the method of nanoindentation is applied to brain tissue slices to identify the effects of swelling on the tissue's mechanical properties. The stiffness and relaxation properties of brain tissue slices are identified, suggesting a useful and simple alternative to *in vivo* imaging for identifying the effects of diseases such as edema or hydrocephalus on the brain.

ACKNOWLEDGEMENTS

I have many individuals to thank who have supported and helped me along the way throughout this project. I would like to first thank my advisor, Professor Yuhang Hu, who guided and challenged me to grow as a graduate student. Thanks to thank my fellow lab mates Dongjing He, Yang Lai, Inkyu Oh, Jiahe Huang, Haohui Zhang, Bohan Wang, and Yunlong Li for our helpful discussions in and out of the lab. Also, I want to thank Dongjing He for helping in analyzing the indentation relaxation results.

I also want to thank those who made this research work possible. Thanks to Ben Peterson and colleagues from the Meat Sciences Laboratory for providing many porcine brain tissue samples to study. Thanks to the Natalie Becerra-Stasiewicz and the MRL staff for the training and use of their facilities to perform indentation testing. Thanks to Dr. Mayandi Sivaguru and the IGB staff for the training and use of their facilities for vibratome sectioning. Lastly, I would like to thank my family and friends for their constant support and encouragement.

TABLE OF CONTENTS

CHAPTER 1: INTRODUCTION

The mechanical nature of brain tissue has only recently come into focus in research as studies on the brain have traditionally been centered on the biochemical and electrophysiological aspects. Understanding the mechanical properties of the brain is now understood to contribute to the development of models important for predicting diseases and identifying the mechanisms underlying brain function. The complexity of brain tissue has made it particularly difficult for researchers to establish a consensus agreement on the structure and function relationship for the behavior of brain tissue [1]. However, since the beginning of experimental studies with regards to the mechanical properties of brain tissue a little over 50 years ago, significant progress has been made due to the advancement of experimental techniques and protocols [2, 3]. By studying the mechanical properties of brain tissue, more comprehensive characterizations and complete models of the brain's behavior can be established. Information derived from mechanical testing will contribute to the development of multiscale and multimodal models, better simulations of brain tissue injury and neurological diseases, as well as opportunities to improve and preserve brain function [4].

Inflammatory reactions in the brain as a primary condition or a secondary condition following incidents of: trauma, hemorrhages, allergies, tumors etc., can commonly cause brain swelling [5]. Abnormal fluid buildup in the brain can lead to life-threatening conditions such as hydrocephalus or more commonly, edema [6]. Brain edema is typically classified as cytotoxic, where cells in the parenchyma swell, or vasogenic, where fluid fills the extracellular spaces [7]. Swelling in the brain is a complicated condition where a better understanding of its pathophysiology and underlying mechanisms are needed to develop effective treatment and management strategies [8]. Treatment of brain edema is commonly done through osmotherapy or

similar techniques that aim to reduce the ICP in the brain, which are limited in effectiveness. In extreme cases, invasive surgery with decompressive craniectomy may be required. To develop effective and novel treatments, the mechanical and molecular mechanisms underlying edema need to be understood [9, 10].

A potential driving force for the mechanism behind brain swelling is a result of the Donnan effect and the triphasic mixture theory [11]. In the healthy physiological state, the brain uses active ion pumps to maintain a delicate balance of ions. When the ion balance is disrupted, or the brain tissue is damaged, water movement can be caused in part, through Donnan osmotic pressure effects [12]. The brain tissue can be considered as a triphasic mixture consisting of a solid matrix (cells and ECM), fluid (water), and solutes (ions and non-permeating solutes), which can freely swell when in an ionic solution [13]. Using tissue slices as an experimental model, the mechanism behind osmotic therapy treatments was shown by swelling brain tissue in different ionic baths [11, 13]. When placed in an ionic solution with an osmolarity greater than the physiological state of 320 mOsm, tissue volume would be reduced as water was drawn out of the tissue. Conversely, tissue volume would increase as water was drawn into the tissue when placed in an ionic solution with an osmolarity lower than 320 mOsm. In these works, the driving forces behind brain tissue swelling are described, but the effect of swelling on the tissue's properties are still lacking.

Studies on brain tissue swelling have focused on identifying the underlying mechanisms [14] and modeling a condition and its effects [15, 16, 17]. In recent years with the development of *in vivo* imaging techniques, MR imaging has been used to study brain swelling and the resulting effects on the shear modulus on the tissue [18]. However, *in vitro* techniques on brain tissue slices remains a simple and alternative method for investigating brain tissue swelling [19].

With recently developed testing techniques for localized measurements, the mechanical properties and brain tissue swelling can be measured.

Many *in vitro* studies have been performed on the tissue level to characterize the behavior of healthy brain tissue. Viscoelastic models have been most commonly used to model the behavior of brain tissue, with early experimental studies utilizing creep [20], relaxation [21, 22], strain rate [23], dynamic shear [24]. The goal of these studies has been to describe and model the behavior of brain tissue. With a better understanding of how testing conditions influence the behavior of brain tissue [25, 26], a standard for testing protocols has been established for preserving brain tissue properties during testing and interstudy comparison. However, due to the intricacies of the brain's structure and the variety of testing conditions, the multiscale behavior of the brain still has not been established.

The improved understanding of mechanical testing on brain tissue has led to more systematic studies to establish models that can effectively capture the behavior of the tissue. Most studies have only modeled the behavior of brain tissue under a singular loading mode, which is not effective for simulating the multiscale and multiple loading modalities present in brain tissue injuries [27]. With systematic testing, efforts have been made to develop a model that can capture the mechanical properties [28] and time-dependent properties [29] of brain tissue under multiple loading conditions. The establishment of such models [30] is addressing the combined loading conditions of brain tissue from tissue-level experiments. To capture the multi-scale response of the tissue, indentation has become a technique utilized in recent years to measure the behavior of brain tissue near the cellular level, able to distinguish between gray matter (mostly neuronal cells) and white matter (mostly axons). Atomic force microscopy (AFM) and indentation have become popular techniques to analyze the local properties of brain

tissue [31, 32, 33], also enabling the *in vitro* mechanical testing of the effects of brain tissue injury [34].

Understanding the effects of swelling on brain tissue will help the development of models to predict and simulate the pathophysiology of diseases such as brain edema and hydrocephalus. Applying indentation to swollen brain tissue is an alternative to the more common and complex *in vivo* imaging studies used to study the effects of swelling in the brain. In this work, brain tissue slices are prepared and swollen in aCSF solution adjusted to different osmolarities. Using nanoindentation, the mechanical and time-dependent properties of swollen brain tissue slices are then examined.

CHAPTER 2: TISSUE PREPARATION AND SWELLING

Porcine brain samples were received from freshly slaughtered pigs at market weight from the Meat Science Laboratory at the University of Illinois Urbana-Champaign. Tissue samples were immediately submerged in an iced solution of artificial cerebrospinal fluid (aCSF) for recovery and neuronal preservation [35]. Samples from the three different anatomical orientations (coronal, sagittal, transverse) were then cut from the brain tissue using a scalpel. Throughout preparation and cutting, the brain tissue (Figure 2.1a) and any contacting surfaces (gloves and scalpel) were constantly hydrated with cold aCSF for tissue preservation. Specimens were then embedded in gelatin for tissue slicing (Figure 2.1b) [36]. Slices 350 μm in thickness were sliced using the Vibratome 1000 Plus Sectioning System, with the vibratome reservoir filled with cold aCSF solution (Figure 2.1c). The vibratome cutting speed was set low at setting 2 and the amplitude was set high at setting 10. Cut tissue slices (Figure 2.1d) were then submerged in cold aCSF solution until testing (within 72 hours postmortem).

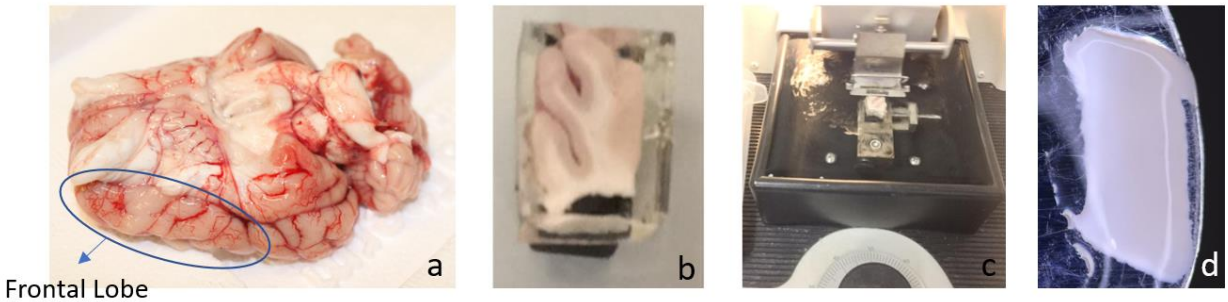

Figure 2.1: The brain tissue preparation process starting from a whole porcine brain from freshly slaughtered pigs. (a) Image of an upside-down whole brain sample. Tissue samples were cut from the circled frontal lobe region. (b) Smaller tissue sections were then embedded in gelatin and mounted on a block using adhesive glue for vibratome slicing. (c) Tissue blocks were mounted on the vibratome and completely covered in cold aCSF solution. (d) Cut tissue slices with thickness of 350 μm.

The aCSF buffer was prepared fresh the day of tissue testing, using deionized water, filtered through a membrane with 0.22 μum pore size, and with (in mM): 126 NaCl, 2 $MgCl_2$, 3 KCl, 1.25 NaH_2PO_4, 2 $CaCl_2$, 26 $NaHCO_3$, 11 glucose and 0.3 kynurenic acid [37]. The buffer's pH was measured and adjusted to 7.35 – 7.40 with NaOH as necessary, and preoxygenated with carbogen gas (95% O_2 + 5% CO_2). The resulting osmolarity was 330±5 mOsm/kg.

The protocol for swelling measurements in brain tissue slices was adapted from Elkin et al. For swelling measurements, gray matter slices from the outer cortex, cut from the frontal lobe in the coronal direction, were used. Slices were swollen at room temperature in aCSF solution for 24 hours. Initial slice thickness and area were then imaged with a macro lens-Nikon DSLR camera, and the volume of the slice determined using ImageJ. Initial weight of each slice was also measured using a mass-balance. Slices were then placed in aCSF solution adjusted to different osmolarities (4 Osm, 2 Osm, 330 mOsm, 100 mOsm, and 6.7 mOsm) using either NaCl to increase the osmolarity, or deionized water to decrease the osmolarity, and allowed to swell to equilibrium overnight. Final slice volume and weight was then measured.

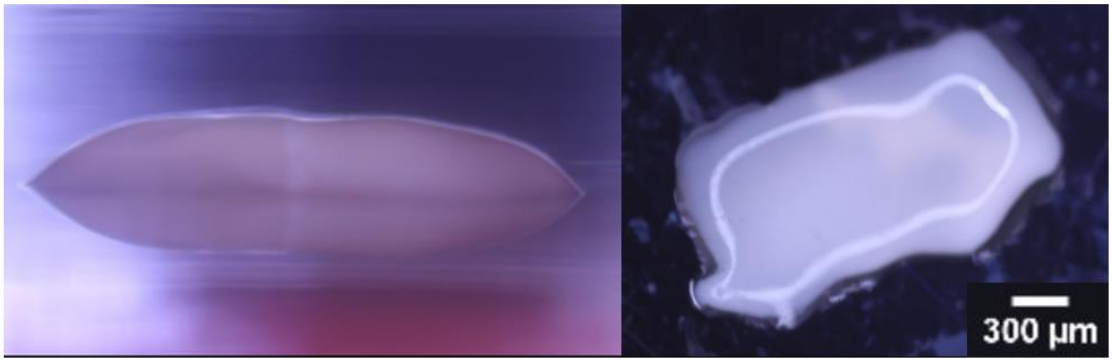

Figure 2.2: Rectangular tissue slices were imaged and weighted. ImageJ was used to calculate the resulting average thickness (left) and area (right) for volume measurements. Images and volume measurements were taken before and after swelling.

The results of swelling in terms of percent weight and volume change of the tissue slices are shown in Figure 2.3. Plotted data are shown as mean value ± standard deviation. The one-way ANOVA test was used to compare the means of the data relative to the isotonic 330 mOsm solution, using a significance level $\alpha = 0.05$. For weight change, only the weight change seen in the 6.7 mOsm solution of 35.5% was significantly different than the isotonic weight change of -3.0%. For volume change, each osmolarity was significantly different than the isotonic solution change (Table 2.1). In the hypertonic solutions, 4 Osm and 2 Osm, tissue slices decreased in weight and volume. In hypotonic solutions, 100 mOsm and 6.7 mOsm, tissue slices increased in weight and volume. This trend follows the results found in Elkin et al., with water flow driven by the Donnan effect resulting in tissue slices losing water in hypertonic solutions and gaining water in hypotonic solutions. Compared to the extreme cases, the 2 Osm and 100 mOsm solutions resulted in significant percent volume changes, but with lower variance. Tissue slices swollen in isotonic 330 mOsm solution, hypertonic 2 Osm solution, and hypotonic 100 mOsm solution, were then used for indentation testing to examine the effects of swelling.

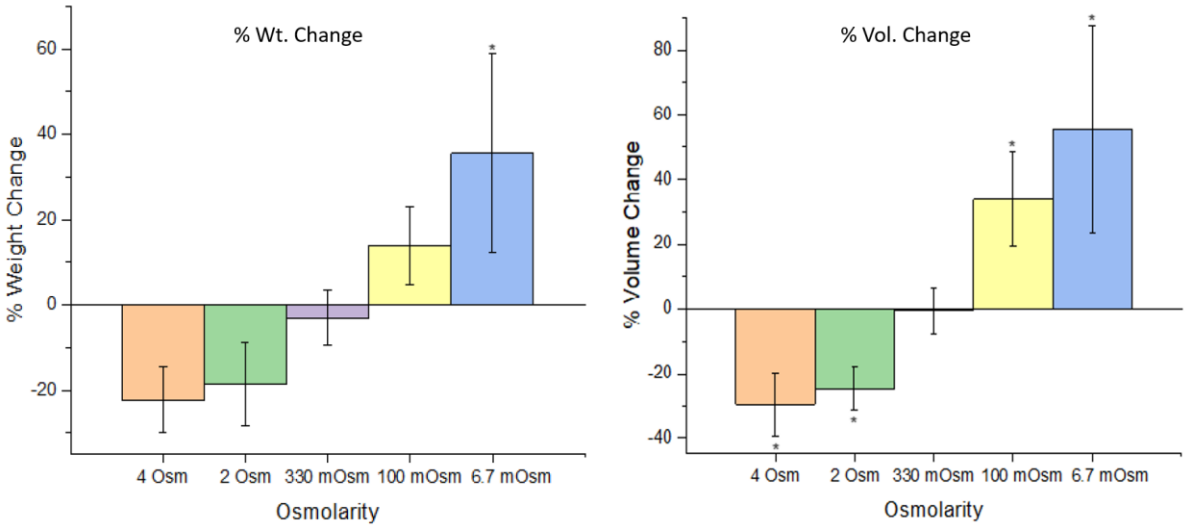

Figure 2.3: The percent weight change (left) and percent volume change (right) after swelling in each solution (4 Osm, 2 Osm, 330 mOsm, 100 mOsm, and 6.7 mOsm). The 330 mOsm aCSF solution is the isotonic solution. $N = 6$ for each solution.

Table 2.1: Percent weight and volume changes of tissue swelling. Average, standard deviation, and statistical significance for each osmolarity are shown. 330 mOsm is taken to be the isotonic condition.

% Weight Change			
	Average	Std. Dev	Significant
4 Osm	-22.3	7.7	No
2 Osm	-18.5	9.7	No
330 mOsm	-3.0	6.5	--
100 mOsm	13.9	9.1	No
6.7 mOsm	35.5	23.3	Yes
% Volume Change			
	Average	Std. Dev	Significant
4 Osm	-29.6	9.8	Yes
2 Osm	-24.6	6.6	Yes
330 mOsm	-0.6	7.2	--
100 mOsm	33.8	14.7	Yes
6.7 mOsm	55.5	32.1	Yes

CHAPTER 3: INDENTATION

3.1 *METHODS*

After swelling, tissue slices were placed into fresh aCSF solution respective to the swelling condition and placed in an ice-bath until testing. The Optics11 Piuma Nanoindenter was used for indentation testing, which has recently been shown to be effective for the testing of biological materials [38, 39, 40]. The Piuma Nanoindenter functions similarly to AFM, by using a cantilever-based probe and fiber-optical interferometry, enabling accurate and precise testing of biological materials. As an alternative to AFM, the Piuma is more robust to liquid testing and is effective for performing indentation testing on multiple samples in quicker fashion.

Before testing, tissue slices were equilibrated to room temperature for at least 30 minutes. The tissue slice surface was first dabbed dry using a Kimwipe, and then mounted on a microscope slide using a thin layer of adhesive. The slide was then mounted onto a petri dish, and the tissue was fully submerged with aCSF solution that matched the osmolarity of the swelling condition (Figure 3.1). For each different osmolarity aCSF solution (2 Osm, 330 mOsm, 100 mOsm), the Piuma signal and probe were recalibrated before testing.

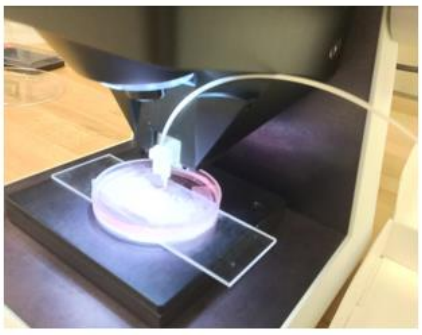

Figure 3.1: Piuma Nanoindenter testing of brain tissue slices submerged in liquid.

Spherical indentation tips (radius 102.5 µm) were used to probe the tissue slice's stiffness and relaxation behavior. For stiffness measurements, specimens were probed to 7 µm in depth, with a loading rate of 5 µm/s (Figure 3.2). For relaxation measurements, specimens were probed to 3 separate indentation depths (5, 10, 15 µm) at each location, with a loading rate of 80 µm/s to minimize loading time and a 10-minute rest period after each indentation for tissue recovery (Figure 3.3 and Figure 3.4). Stiffness measurements were taken at locations spaced at least 100 µm apart, and relaxation measurements were taken at locations spaced at least 1000 µm apart.

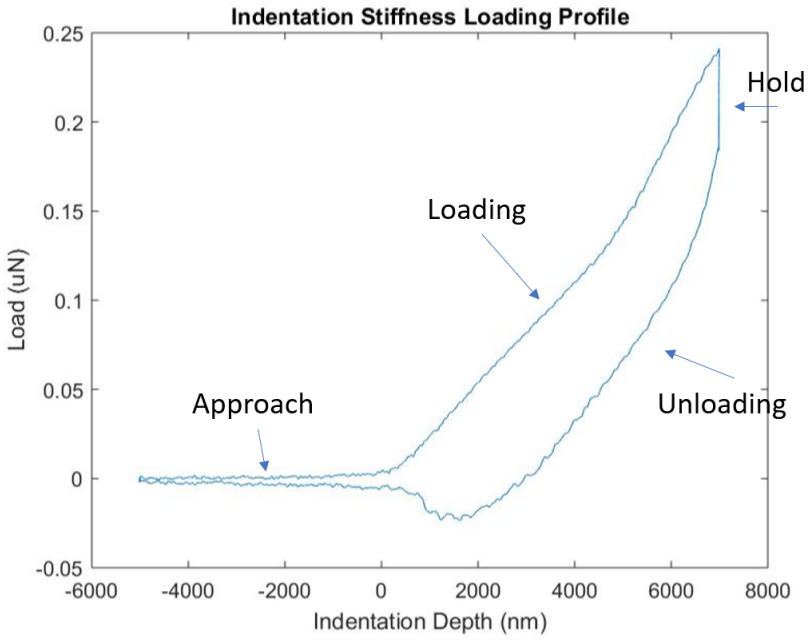

Figure 3.2: Loading profile for stiffness measurements. The probe approaches the surface, indents the specimen to a depth of 7 µm, holds for 1 second, and then unloads.

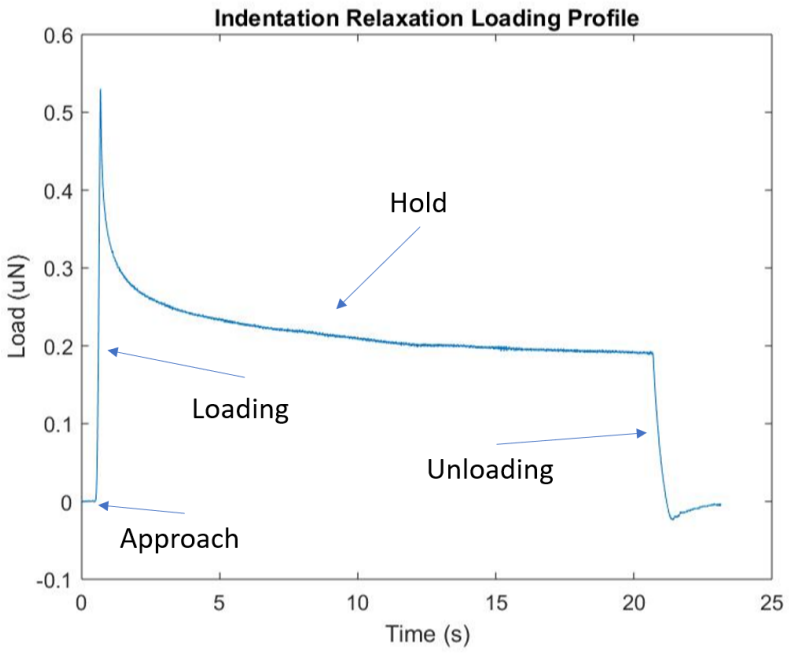

Figure 3.3: Loading profile for relaxation measurements. The probe approaches the surface, lowers to the set indentation depth (5, 10, or 15 μm), holds for 20 seconds, and then unloads.

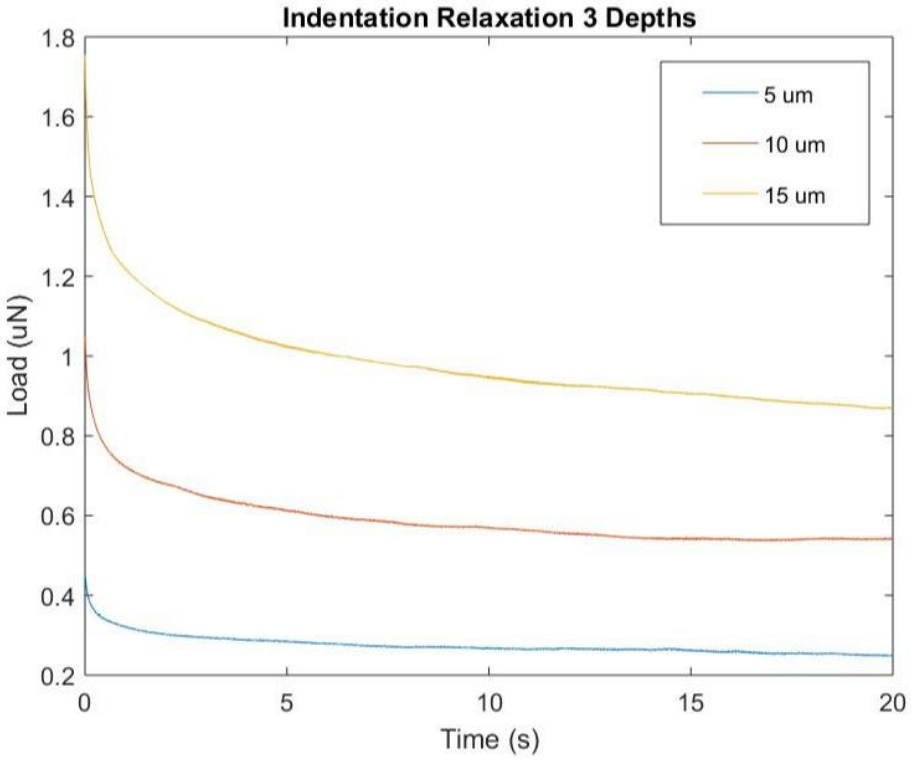

Figure 3.4: Representative plots of 3 relaxation indentation measurements at 1 location. Before each indentation, there was a 10-minute rest time.

3.2 *STIFFNESS*

Indentation tests for stiffness were performed on brain tissues to examine the effects of orientation from which tissue slices were cut (coronal, sagittal, transverse), location (gray matter vs. white matter), and swelling in aCSF solutions at different osmolarities (hypertonic, isotonic, hypotonic). A total of 123 indentation tests for stiffness, averaging to around n = 7 for each orientation, location, and osmolarity. By analyzing the indentation profile (Figure 3.2), the Hertz model was applied to determine the effective Young's modulus, E, of each sample [40]. For each loading curve, the data up to 60% of the peak applied load was used for determining E through Equation 3.1, where P is the applied load, R is the radius of the indenter, and h is the indentation depth. The data are then plotted as mean value ± standard deviation. As in the swelling measurements, the one-way ANOVA test was used to compare the means of the data, using a significance level $\alpha = 0.05$.

$$P = \frac{4}{3} E * R^{\frac{1}{2}} * h^{\frac{3}{2}} \qquad (3.1)$$

To examine anisotropy in the brain tissue, data were plotted to examine orientation in gray matter, GM, (Figure 3.5 left) and white matter, WM, (Figure 3.5 right). Generally, tissue slices from the sagittal direction, S, were less stiff compared to the coronal, C, and transverse, T, directions. The S direction being less stiff is seen in the 330 mOsm GM, 100 mOsm GM, 2 Osm WM, and 330 mOsm WM conditions. For the other 2 conditions of 2 Osm GM and 100 mOsm WM, the T and C directions were least stiff, respectively (Table 3.1). Anisotropy is observed in the brain tissue slices across both GM and WM in each osmolarity. Slices cut along the S direction tended to be least stiff relative to the C and T directions; however, for 2 Osm GM and 100 mOsm WM, the T and C directions had an even lower average stiffness respectively. Due to the high variance and low statistical stiffness among the orientations, additional tests would need

to be conducted to draw significant conclusions. However, the trend of these results agrees with the complexity of the structure in brain tissue. GM is generally viewed as isotropic, but in this case, anisotropic behavior is expected due to localized structural differences and from variance in the local measurements on the samples due to handling and preparation methods.

To examine the effects of location, data were plotted (Figure 3.6) in groups of 2 and tabulated (Table 3.2) to compare the stiffness of GM verses WM. For all orientations and osmolarities except for 330 mOsm T and 100 mOsm C, WM was stiffer than GM. In every osmolarity and orientation except for 330 mOsm T and 100 mOsm C, WM was stiffer than GM. This general trend of WM being stiffer than GM is expected due to the myelination of axons, which greatly contributes to the stiffness of the tissue. Depending on the orientation of the fibers and other contributing factors in the brain tissue's structure, it is expected that under some orientations and swelling conditions, GM may be stiffer than WM, which is observed in 330 mOsm T and 100 mOsm C.

To examine the effects of osmolarity and swelling the data were plotted in groups of 3 for comparison (Figure 3.7) and the changes from the isotonic conditions are tabulated (Table 3.3). In each orientation and location tested, swelling in hypertonic and hypotonic solutions reduced the stiffness of the tissue relative to the isotonic condition. The decrease in stiffness was more pronounced in the hypertonic solutions than in the hypotonic solutions, with an average decrease of 37.2% and 25.1% respectively. The overall trend of the tissue decreasing in stiffness with swelling in non-isotonic solution is supported due to swelling often acting as a secondary source of damage to the tissue (i.e. swelling following a TBI incident), damaging the structure and reducing the stiffness of the tissue.

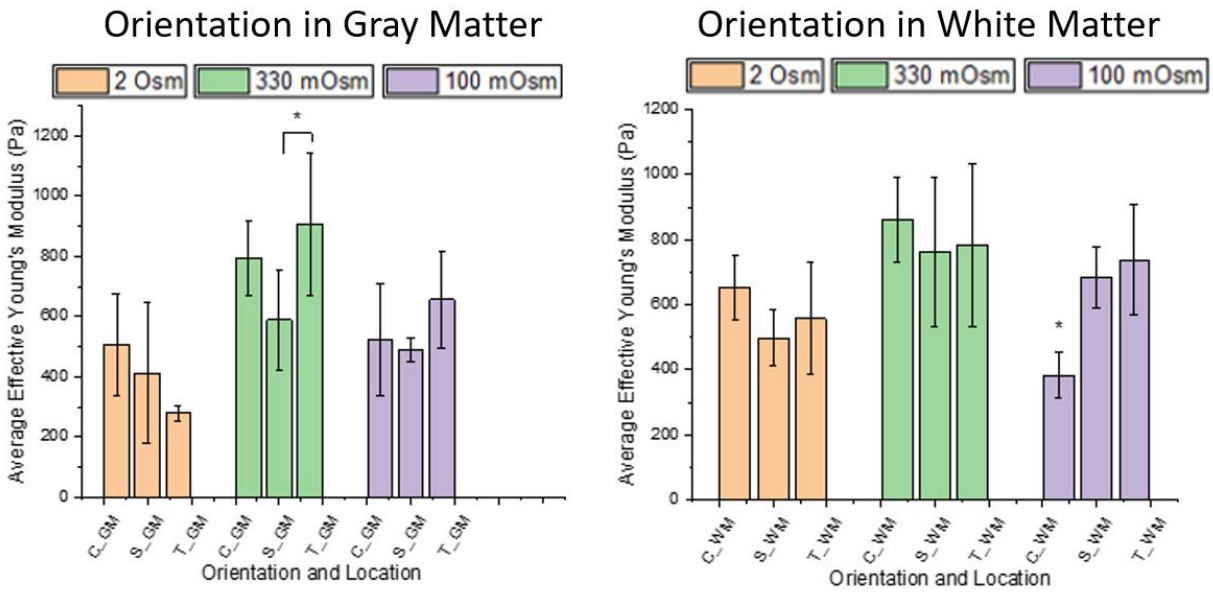

Figure 3.5: Indentation stiffness data grouped to compare effect of orientation.

Table 3.1: Orientation with the lowest average E compared to the other 2 orientations for each test condition tested.

	Orientation with Lowest Average E (Pa)	Average E (Pa) of other 2 orientations
2 Osm GM	280.1 (T)	463.7
330 mOsm GM	588.9 (S)	853.9
100 mOsm GM	490.0 (S)	583.5
2 Osm WM	498.0 (S)	601.5
330 mOsm WM	761.3 (S)	831.4
100 mOsm WM	382.4 (C)	702.7

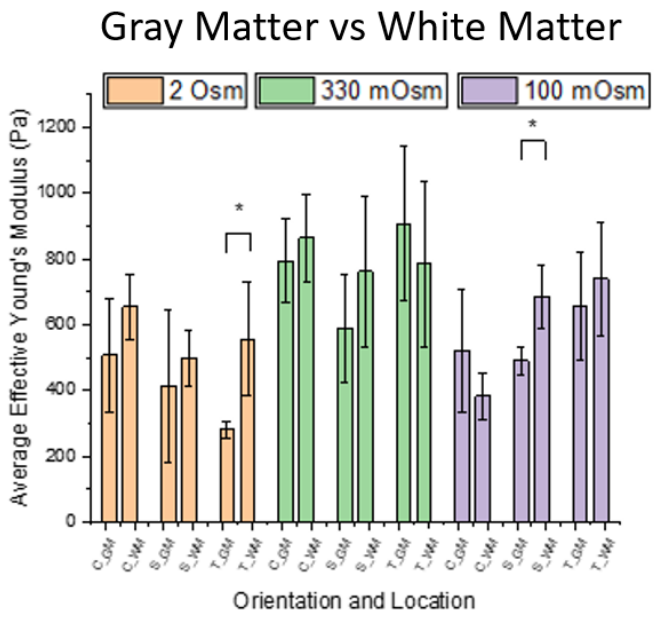

Figure 3.6: Indentation stiffness data grouped to compare effect of location.

Table 3.2: Comparison of stiffness in locations for each orientation and osmolarity.

	E (Pa) of GM	E (Pa) of WM	Stiffer Region
2 Osm C	506.3	654.8	WM
2 Osm S	412.7	498.0	WM
2 Osm T	280.1	557.0	WM
330 mOsm C	794.5	862.9	WM
330 mOsm S	588.9	761.3	WM
330 mOsm T	906.7	783.97	GM
100 mOsm C	521.0	382.4	GM
100 mOsm S	490.0	684.8	WM
100 mOsm T	656.4	738.6	WM

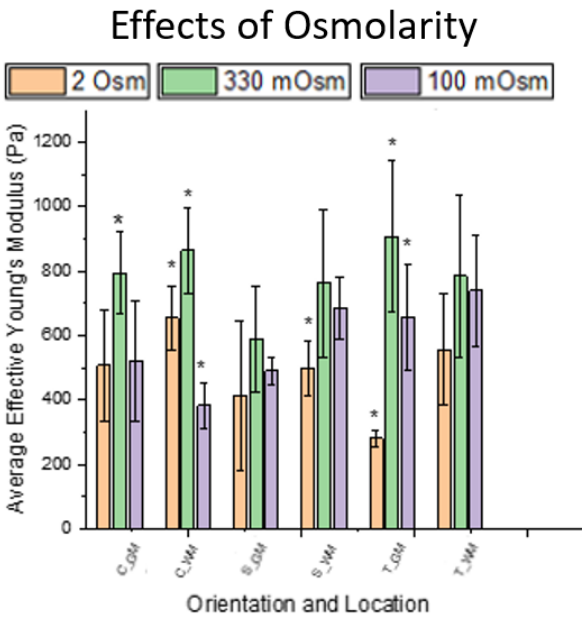

Figure 3.7: Indentation stiffness data grouped to compare the effects of osmolarity and swelling.

Table 3.3: Comparison of effects of osmolarity on tissue stiffness.

Stiffness in Pa (% Change from Isotonic Condition)	Hypertonic 2 Osm	Isotonic 330 mOsm	Hypotonic 10 mOsm
C GM	506.3 (-36.3%)	794.5	521.0 (-34.4%)
C WM	654.8 (-24.1%)	862.9	382.4 (-55.7%)
S GM	412.7 (-29.9%)	588.9	490.0 (-16.8%)
S WM	498.0 (-34.6%)	761.3	684.8 (-10.0%)
T GM	280.1 (-69.1%)	906.7	656.4 (-27.6%)
T WM	557.1 (-28.9%)	784.0	738.6 (-5.8%)

3.3 *RELAXATION*

For each swelling condition (hypertonic, isotonic, hypotonic), orientation (C, S, T), and location (GM, WM), 6 sets of 3 separate indentation measurements to different depths (5 μm, 10 μm, 15 μm) were taken and averaged together. A total of n = 324 individual relaxation indentation tests were performed. The brain tissue is assumed to be an incompressible, viscoelastic material, where the relationship between the relaxation modulus and force is given by Equation 3.2 [41]. P is the reaction force, R is the radius of indenter, h_0 is the indentation depth, and G is the relaxation modulus.

$$P(t) = \frac{8\sqrt{R}}{3} h_0^{\frac{3}{2}} G(t) \qquad (3.2)$$

To examine the viscoelastic behavior, the shear relaxation modulus ratio, g_i, and the relaxation time constant, τ_i, are determined by fitting with a 2-term Prony series in MATLAB (Equation 3.3). A representative plot of an experimental data set and Prony series fit are shown in Figure 3.8.

$$G(t) = G_0\left(1 - \sum_{i=1}^{2} g_i \left[1 - e^{-\frac{t}{\tau}}\right]\right) \qquad (3.3)$$

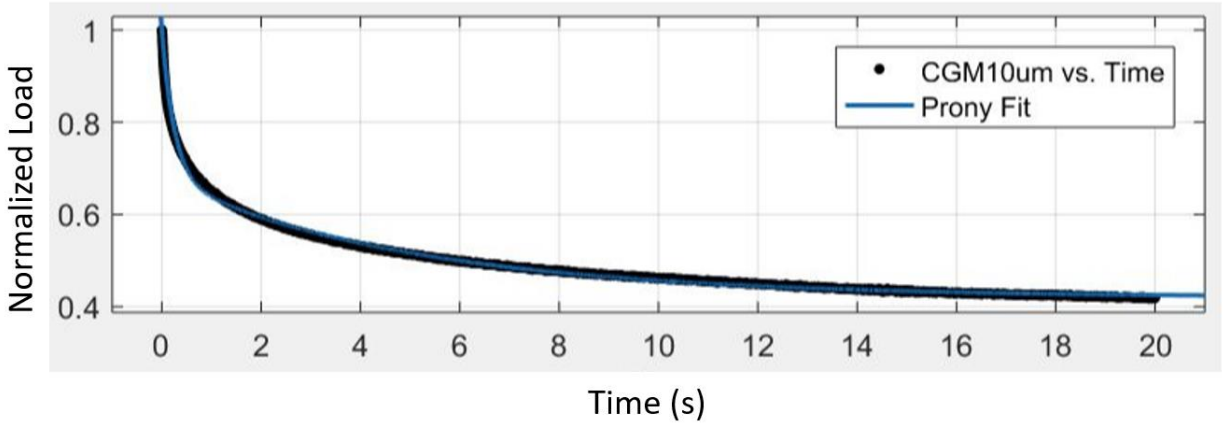

Figure 3.8: Representative plot of experimental data and theoretical fit for an indentation relaxation test.

To first compare the effects of swelling, the ratios and constants were averaged within each solution (Table 3.4). Relative to the isotonic solution, both the hypertonic (2 Osm) and hypotonic (100 mOsm) solutions have increased g_i and decreased τ_i. This indicates that the tissue slices in the isotonic solutions are relaxing to a greater degree and more slowly than those in the non-isotonic solutions. The slices in non-isotonic solutions underwent further swelling, which likely added damage to its structure and decreased its stiffness as shown above (Figure 3.7 and Table 3.3). The slices in the isotonic solution would have a structure that more resembles its healthy physiological state, with neurons and axons retaining more of their structural integrity, which likely causes them to relax with greater time constants than in the non-isotonic condition.

The effects of indentation depth, with values across all the conditions averaged by depth, are shown in Table 3.5. With increasing depth, g_1 decreased, and τ_i increased. By increasing the indentation depth, a greater volume of brain tissue is deformed, which would lead to greater relaxation on a slower time scale. The effects of location were varied in g_1 and g_2, but with τ_i being greater in GM (Table 3.6). This indicates that the neurons that primarily consist of the structure in GM relax slower than the axons that primarily consist of the structure in WM. The effects of orientation are shown in Table 3.7. The parameters across the S and T orientations are similar, with the g_i values being nearly identical, and with the τ_i in the S orientation being slightly below those in the T orientation. However, the C orientation here is different with lower g_i and greater τ_i values, indicating anisotropy (converse to the S orientation indicating anisotropy when comparing stiffness values).

Table 3.4: Parameters averaged within each solution.

	g_1	g_2	τ_1 (s)	τ_2 (s)
2 Osm	0.40	0.21	0.15	4.64
330 mOsm	0.30	0.19	0.22	5.51
100 mOsm	0.35	0.23	0.19	4.40

Table 3.5: Parameters averaged by indentation depth.

	g_1	g_2	τ_1 (s)	τ_2 (s)
5 µm	0.37	0.17	0.10	3.77
10 µm	0.35	0.23	0.20	4.93
15 µm	0.33	0.23	0.25	5.85

Table 3.6: Parameters averaged by location.

	g_1	g_2	τ_1 (s)	τ_2 (s)
GM	0.32	0.22	0.21	5.4
WM	0.38	0.20	0.16	4.3

Table 3.7: Parameters averaged by orientation.

	g_1	g_2	τ_1 (s)	τ_2 (s)
C	0.33	0.21	0.21	5.21
S	0.36	0.21	0.16	4.47
T	0.36	0.21	0.19	4.86

CHAPTER 4: CONCLUSION AND FUTURE WORK

Swelling in brain tissue slices was first demonstrated using hypertonic, isotonic, and hypotonic solutions. Relative to the isotonic condition, slices in hypertonic solutions swelled by decreasing in weight and volume. Slices in hypotonic solutions swelled by increasing in weight and volume. Tissue slices swollen to equilibrium were then tested with nanoindentation for their stiffness and viscoelastic relaxation behavior. From the stiffness results, anisotropy was observed with slices from the sagittal direction being least stiff. White matter locations were observed to be stiffer than gray matter locations. Swelling in hypertonic and hypotonic solutions reduced the stiffness of the tissue relative to the isotonic condition. However, additional measurements are needed to reduce the variance observed between groups when comparing stiffness, and for the results to be more statistically significant. From the relaxation results, a 2-term Prony series was used to fit the data and extract viscoelastic parameters g_i and τ_i. Swelling in hypertonic and hypotonic solutions led to the tissue slices relaxing quicker with a smaller decrease in modulus. Compared to gray matter, white matter slices relaxed less and relaxed on a quicker time scale. As opposed to the sagittal orientation indicating anisotropy when observing stiffness, the coronal orientation indicated anisotropy when observing the viscoelastic parameters.

Future studies include additional indentation measurements to produce more statistically significant results. Additionally, tissue slices would have their structure imaged before indentation testing with Diffusion Tensor Imaging to confirm fiber orientation, and after indentation testing with histology to gain insight into how the swelling treatment affected the tissue's structural integrity on the cellular level. With the useful alternative of performing *in vitro* experiments to study brain tissue swelling, the next steps also include incorporating the measured mechanical properties into a model to predict and simulate swelling in the brain.

REFERENCES

[1] A. Goriely, M.G.D. Geers, G.A. Holzapfel, J. Jayamohan, A. Jérusalem, S. Sivaloganathan, W. Squier, J.A.W. van Dommelen, S. Waters, E. Kuhl, "Mechanics of the brain: perspectives, challenges, and opportunities," *Biomech Model Mechanobiol*, vol 14, pp. 931-965, 2015.

[2] A.K. Ommaya, "Mechanical properties of tissues of the nervous system," *J. Biomechanics*, vol 1, pp. 127-138, 1968.

[3] S. Chatelin, A. Constantinesco, R. Willinger, "Fifty years of brain tissue mechanical testing: from in vitro to in vivo investigations," *Biorheology*, vol. 47, pp. 255-276, 2010.

[4] N. Antonovaite, S.V. Beekmans, E.M. Hol, W.J. Wadman, D. Iannuzzi, "Regional variations in stiffness in live mouse brain tissue determined by depth-controlled indentation mapping," *Scientific Reports*, vol. 8, pp. 1-11, 2018.

[5] D. Adukauskienė, A. Bivainytė, E. Radavičiūtė, "Cerebral edema and its treatment," *Medicina*, vol. 43, pp. 170-176, 2007.

[6] G.E. Lang, D. Vella, S.L. Waters, A. Goriely, "Propagation of damage in brain tissue: coupling the mechanics of oedema and oxygen delivery," *Biomech Model Mechanobiol*, vol. 14, pp. 1197-1216, 2015.

[7] I. Klatzo, "Pathophysiological aspects of brain edema," *Acta Neuropathol*, vol. 72, pp. 236-239, 1987.

[8] A.W. Unterberg, J. Stover, B. Kress, K.L. Kiening, "Edema and brain trauma," *Neuroscience*, vol. 129, pp. 1021-1029, 2004.

[9] S.K. Jha, "Cerebral edema and its management," *Medical Journal Armed Forces India*, vol. 59, pp. 326-331, 2003.

[10] J.M. Simard, J. Badaut, N. Plesnila, “Perspectives on future translational research on brain edema,” *Brain Edema,* ch. 25, pp. 497-505, 2017.

[11] B.S. Elkin, M. A. Shaik, B. Morrison III, “Fixed negative charge and the donnan effect: a description of the driving forces associated with brain tissue swelling and oedema,” *Phil Trans R Soc A,* vol. 368, pp. 585-603, 2010.

[12] N.O. Chahine, F.H. Chen, C.T. Hung, G.A. Ateshian, “Direct measurement of osmotic pressure of glycosaminoglycan solutions by membrane osmometry at room temperature,” *Biophysical Journal,* vol. 89, 2005.

[13] G.E. Lang, P.S. Stewart, D. Vella, S.L. Waters, A. Goriely, “Is the Donnan effect sufficient to explain swelling in brain tissue slices?” *J R Soc Interface,* vol. 11, 2014.

[14] T. Donato, Y. Shapira, A.Artru, K. Powers, “Effect of mannitol on cerebrospinal fluid dynamics and brain tissue edema,” *J Anesth Analg,* vol. 78, pp. 58-66, 1994.

[15] P.J. Basser, “Interstitial pressure, volume, and flow during infusion into brain tissue,” *Microvascular Research,* vol. 44, pp. 143-165, 1992.

[16] Z. Taylor, K. Miller, “Reassessment of brain elasticity for analysis of biomechanisms of hydrocephalus”, *J Biomechanics,* vol. 37, pp. 1263-1269, 2004.

[17] T. Nagashima, N. Tamaki, S. Matsumoto, B. Horwitz, Y. Seguchi, “Biomechanics of hydrocephalus: a new theoretical model,” *Neurosurgery,* vol. 21, pp. 898-904, 1987.

[18] S.A. Kruse, G.H. Rose, K.J. Glaser, A. Manduca, J.P. Felmlee, C.R. Jack Jr., R.L. Ehman, “Magnetic resonance elastography of the brain,” *NeuroImage*, vol. 39, pp. 231-237, 2007.

[19] S. Cho, A. Wood, M.R. Bowlby, “Brain slices as models for neurodegenerative disease and screening platforms to identify novel therapeutics,” *Current Neuropharmacology*, vol. 5, pp. 19-33, 2007.

[20] M.C.H. Dodgson, “Colloidal structure of brain,” *Biorheology,* vol. 1, pp. 21-30, 1962.

[21] J.E. Galford, J.H. McElhaney, “A viscoelastic study of scalp, brain, and dura,” *J Biomechanics,* vol. 3, pp. 211-221, 1970.

[22] K.B. Arbogast, D.F. Meaney, L.E. Thibault, “Biomechanical characterization of the constitutive relationship for the brainstem,” *SAE International*, 1995.

[23] K. Miller, K. Chinzei, “Constitutive modelling of brain tissue: experiment and theory,” *J Biomechanics,* vol. 30, pp. 1115-1121, 1997.

[24] G.T. Fallenstein, V.D. Hulce, “Dynamic mechanical properties of human brain tissue,” *J Biomechanics,* vol. 2, pp. 217-226, 1969.

[25] F. Pervin, W.W. Chen, “Effect of inter-species, gender, and breeding on the mechanical behavior of brain tissue,” *NeuroImage*, vol. 54, pp. S98-S102, 2011.

[26] M. Hrapko, J.A.W. van Dommelen, G.W.M. Peters, J.S.H.M. Wismans, “The influence of test conditions on characterization of the mechanical properties of brain tissue,” *J Biomechanical Engineering*, vol. 130, pp. 031003-1-10, 2008.

[27] D.F. Meaney, B. Morrison, C.D. Bass, “The mechanics of traumatic brain injury: a review of what we know and what we need to know for reducing its societal burden,” *J Biomechanical Engineering*, vol. 136, pp. 021008-1-14, 2014.

[28] S. Budday, G. Sommer, C. BIrkl, C. Langkammer, J. Haybaeck, J. Kohnert, M. Bauer, F. Paulson, P. Steinmann, E. Kuhl, G.A. Holzapfel, “Mechanical characterization of human brain tissue,” *Acta Biomterialia,* vol. 48, pp. 319-340, 2017.

[29] S. Budday, G. Sommer, J. Haybaeck, P. Steinmann, G.A. Holzapfel, E. Kuhl, “Rheological characterization of human bran tissue,” *Acta Biomaterialia*, vol. 60, pp. 315-329, 2017.

[30] L.A. Mihai, S. Budday, G.A. Holzapfel, E. Kuhl, A. Goriely, “A family of hyperelastic models for human brain tissue,” *J Mechanics Physics Solids,* vol. 106, pp. 60-79, 2017.

[31] B.S. Elkin, E.U. Azeloglu, K.D. Costa, B. Morrison III, “Mechanical heterogeneity of the rat hippocampus measured by atomic force microscope indentation,” *J Neurotrauma,* vol. 24, pp. 812-822, 2007.

[32] J.A.W. van Dommelen, T.P.J. van der Sande, M. Hrapko, G.W.M. Peters, “Mechanical properties of brain tissue by indentation: interregional variation,” *J Mechanical Behavior Biomedical Materials,* vol. 3, pp. 158-166, 2010.

[33] S. Budday, R. Nay, R. de Rooji, P. Steinmann, T. Wyrobek, T.C. Ovaert, E. Kuhl, “Mechanical properties of gray and white matter brain tissue by indentation,” *J Mechanical Behavior Biomedical Materials,* vol. 46, pp. 318-330, 2015.

[34] E. Moeendarbary, I.P. Weber, G.K. Sheridan, D.E. Koser, S. Soleman, B. Haenzi, E.J. Bradbury, J. Fawcett, K. Franze, “The soft mechanical signature of glial scars in the central nervous system,” *Nature Communications,* vol. 8, pp. 1-11, 2017.

[35] J.T. Ting, B.R. Lee, P. Chong, G. Soler-Llavina, C. Cobbs, C. Koch, H. Zeng, E. Lein, “Preparation of acute brain slices using an optimized n-methyl-d-glucamine protective recovery method”, *J Visualized Experiments*, pp. 1-13, 2018.

[36] K.I. Kapelsohn, “Improved methods for cutting, mounting, and staining tissue for neural histology,” *Protocol Exchange*, 2015.

[37] X. Wu, M. Mathuchamy, D.S. Reddy, “Atomic force microscopy protocol for measurement of membrane plasticity and extracellular interactions in single neurons in epilepsy,” *Front Aging Neurosci*, vol. 8, 2016.

[38] E. Amann, P. Wolff, E. Breel, M. van Griensven, E.R. Balmayor," Hyaluronic acid facilitates chondrogenesis and matrix deposition of human adipose derived mesenchymal stem cells and human chondrocytes co-cultures," *Acta Biomaterialia*, vol. 52, pp. 130-144, 2017.

[39] T.H. Qazi, D.J. Mooney, G.N. Duda, S. Geissler, "Biomaterials that promote cell-cell interactions enhance the paracrine function of MSCs," *Biomaterials*, vol. 140, pp. 103-114, 2017.

[40] G. Mattei, N. Looze, E.J. Breel, "Measuring micro-mechanical properties of (bio)materials by nano-indentation," *Optics11,* 2017.

[41] J.M Mattice, A. G. Lau, M.L. Oyen, R.W. Kent, "Spherical indentation load-relaxation of soft biological tissues," *J Materials Research,* vol. 8, pp. 2003-2010, 2006.